Germanium-based quantum emitters towards a time-reordering entanglement scheme with degenerate exciton and biexciton states

Nicola Dotti,[1] Francesco Sarti,[1] Sergio Bietti,[2] Alexander Azarov,[3] Andrej Kuznetsov,[3] Francesco Biccari,[1] Anna Vinattieri,[1] Stefano Sanguinetti,[2] Marco Abbarchi,[4,*] and Massimo Gurioli[1,*]

[1]*LENS, Dipartimento di Fisica, Università di Firenze, Via Sansone 1, I-50019 Sesto Fiorentino, Italy*

[2]*L-NESS and Dipartimento di Scienza dei Materiali, Università di Milano Bicocca, Via Cozzi 53, I-20125 Milano, Italy*

[3]*Department of Physics, University of Oslo, NO-0316 Oslo, Norway*

[4]*CNRS, Aix-Marseille Université, Centrale Marseille, IM2NP, UMR 7334, Campus de St. Jérôme, 13397 Marseille, France*

(Received 16 January 2015; revised manuscript received 7 May 2015; published 29 May 2015)

We address the radiative emission of individual germanium extrinsic centers in $Al_{0.3}Ga_{0.7}As$ epilayers grown on germanium substrates. Microphotoluminescence experiments demonstrate the capability of high temperature emission (70 K) and complex exciton configurations (neutral exciton X and biexciton XX, positive X^+ and negative X^- charged excitons) of these quantum emitters. Finally, we investigate the renormalization of each energy level showing a large and systematic change of the binding energy of XX and X^+ from positive to negative values (from $\sim+5$ meV up to ~-7 meV covering $\sim$70 meV of the emission energy) with increasing quantum confinement. These light emitters, grown on a silicon substrate, may exhibit energy-degenerate X and XX energy levels. Furthermore, they emit at the highest detection efficiency window of Si-based single-photon detectors. These features render them a promising device platform for the generation of entangled photons in the *time-reordering scheme*.

DOI: 10.1103/PhysRevB.91.205316 PACS number(s): 71.35.−y, 71.55.−i, 71.70.Gm, 78.55.−m

I. INTRODUCTION

The implementation of quantum states of light is at the base of most quantum computation and quantum information protocols [1–3]: bright and high-quality single-, entangled-, and indistinguishable-photon emitters are a necessary resource for quantum key distribution, quantum repeaters, and photonic quantum information processing [4–7]. In the same field, other important applications of solid-state quantum sources consist in the possibility to couple them with atomic vapors for the production of quantum bits based on slow-light memories [8,9] or on electron and hole spins [10–12]. Single-photon emission [13,14] has been demonstrated in several solid-state systems such as epitaxial and colloidal quantum dots [15–29], carbon nanotubes [30], and single molecules [31–33].

More advanced implementations of quantum states of light, such as entangled photon pairs, can be obtained in solid-state systems, provided the binding of two correlated electronic states within the same nanostructure [4,15,20,26–28,34]. Several schemes for the generation of entangled photons have been proposed for quantum dots. Most of them are based on the neutral biexciton-exciton cascade XX-X: provided the implementation of a spin-degenerate neutral exciton transition, a maximally entangled photon pair can be encoded in the polarization degree of XX and X photons. The requirement of spin degeneracy can be satisfied for negligible electron-hole spin interaction allowing one to erase the *which-path information* in the biexciton-exciton cascade. This kind of spin-degenerate state has been implemented either as an *a priori*, built-in characteristic of the nanostructure (like in Ref. [26] where highly symmetric and unstrained quantum dots were grown [35–37]), by spectral filtering the photons having the same energy [38], or by tuning *a posteriori* the fine interaction to zero [20,25,28,34].

A different protocol called *time-reordering scheme*, has been recently proposed in order to implement polarization entanglement in the emitted photon cascade (XX-X) from quantum dots (QDs) with arbitrary spin splitting [39,40]. This scheme is based on the zero biexciton binding energy allowing one to erase the *which-path information* by introducing *a posteriori* and *ad hoc* delay of the XX-X emitted photons. The time-reordering protocol relaxes the need of a perfectly spin-degenerate neutral exciton state, but the condition of zero biexciton binding energy is not straightforward to be realized, and this photon entanglement scheme has not yet been experimentally demonstrated. Still there are a few reports on QDs naturally exhibiting degenerate XX and X states [41–44] or on the possibility of tuning *a posteriori* the XX binding energy to zero with an external control [25,28,34].

A second relevant route to obtain quantum light sources in semiconductor devices as an alternative to conventional QDs, is related to the exploitation of extrinsic centers in III-V, IV, and II-VI semiconductor alloys [45–48]. Single-photon emission from isolated impurity centers has been shown in ZnSe/ZnMgSe alloys [49], tellurium isoelectronic dyads in ZnSe [50], nitrogen impurity centers in GaAs [51–54] and in AlAs [55], and with nitrogen-vacancy centers and chromium in diamonds [52,56–61].

Within this class of quantum emitters, some impurity centers (for example, dyad complexes [50,55]) allow one to confine exciton complexes, thus leading to the possibility to be exploited as sources of entangled photons. Nevertheless, for extrinsic centers, the scientific literature on the XX-X cascade is much less flourished with respect to QDs and, for example, the possibility to obtain time-reordering has not yet been reported. Among several interesting features, a peculiar property of extrinsic centers is the possibility to exploit them in indirect band-gap-based devices, such as carbon [62,63]

*Corresponding authors: marco.abbarchi@im2np.fr; gurioli@fi.infn.it

and copper [64,65] impurity centers in silicon and carbon antisite-vacancy pairs in SiC [66]. This last example has been demonstrated to be a bright single-photon emitter at room temperature.

In a recent paper, we showed a hybrid III-V/IV-IV single-photon device based on extrinsic emitters in $Al_{0.3}Ga_{0.7}As$ [67] fabricated with a low thermal budget method on Ge and Si substrates, thus providing a solid-state platform towards the integration of quantum light sources in *classical* electronic devices.

In this paper, we first unambiguously demonstrate, by a comparative analysis with samples grown in different conditions, the connection of these latter extrinsic emitters [67] with Ge contamination of the $Al_{0.3}Ga_{0.7}As$ alloy. Then, by a careful microphotoluminescence analysis we are able to image a large sample region isolating a large ensemble of extrinsic defects and determining their density and *pseudo-macrophotoluminescence* spectrum. We also perform a statistical analysis of the excitonic complexes from these Ge centers, demonstrating the change from binding to antibinding of the biexciton XX and positive charged exciton X^+ states with the increase of the emission energy of the corresponding neutral exciton transition X, thus opening the possibility to implement a time-reordering scheme for the XX-X photon cascade exploiting defects in semiconductors. We finally validate their photostability at high temperature and show a selective quantum-confined Stark effect as the main origin of the different inhomogeneous line broadening of the s-shell bright states (the two neutral states X and XX, plus the positive and negative charged excitons, X^+ and X^-, respectively). It is important to note that the devices in use were grown on standard Ge substrates and they emit in the spectral interval of highest detection efficiency of most single-photon silicon-based light detectors.

The paper is organized as follows: In Sec. II we provide a description of the experimental setup used for the microphotoluminescence (micro-PL) investigation and the sample fabrication. In Sec. III we precisely address the origin of the extrinsic centers as Ge-related defects, comparing purely III-V (Ge-free samples) with samples grown on a germanium substrate. In addition we map the Ge-centers emission over large areas thus enabling the precise isolation of the related *pseudo-macro-PL* ensemble emission. In Sec. IV the high-power excitation regime is discussed showing the onset of multiexcitonic and charged exciton features. We also discuss the photostability at high temperature of individual Ge centers as well as the quantum-confined Stark effect originated from charged defects in the surrounding semiconductor matrix. Finally, in Sec. V, we discuss the features of the binding energy of XX, X^+ and X^- showing the transition from binding to antibinding of XX and X^+. In Sec. VI we draw the conclusions.

II. EXPERIMENTAL: SAMPLE PREPARATION AND EXPERIMENTAL METHODS

A thorough description of the device in use can be found in Refs. [67,68] where the first evidence of excitonic recombination and single-photon emission were shown for Ge impurities in $Al_{0.3}Ga_{0.7}As$ grown on germanium and silicon

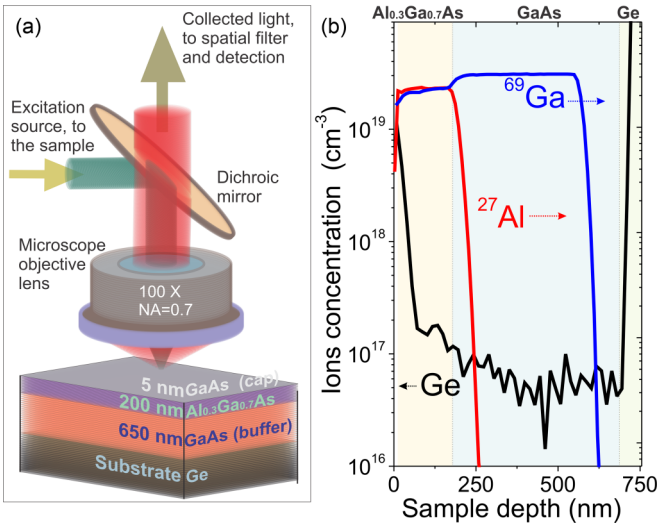

FIG. 1. (Color online) (a) Bottom: Sketch of the sample composition: 5 nm GaAs (capping layer), 200 nm $Al_{0.3}Ga_{0.7}As$ (active layer), 650 nm GaAs (buffer layer), Ge (substrate). Top: Scheme of the optical apparatus used for PL experiments. (b) SIMS measurements on the investigated sample. Ge (left axis, calibrated), Ga and Al (right axis, not calibrated) ions concentration are plotted in a logarithmic scale as a function of the milled depth. Shaded areas highlight the different layers.

substrates. The results found for the two different kinds of substrates are very similar and here we concentrate our attention only on the Ge-substrate case. A scheme of the sample cross section is given in the bottom part of Fig. 1(a) (this sample will be denoted as Ge 580 °C in the following).

As references, we grew two test samples with similar parameters of those described before but on conventional GaAs substrates and, in one case, also using low temperature growth in order to facilitate possible Al clustering. For the first test sample on GaAs we grew a 200 nm $Al_{0.3}Ga_{0.7}As$ layer at 580 °C for the first 100 nm, 400 °C for the central 30 nm, and again 580 °C for the last 70 nm (this sample will be denoted as GaAs 400 °C in the following). In the second test sample the temperature was set at 580 °C for the full 200 nm $Al_{0.3}Ga_{0.7}As$ thickness (this sample will be denoted as GaAs 580 °C in the following).

For micro-PL experiments the samples were kept at low temperature in a low-vibration liquid He-flow cold-finger cryostat which in turn was mounted on a stepping motor translation stage for scanning the sample surface. A schematic view of the experimental setup is shown in the top part of Fig. 1(a). More details are given in Refs. [67,68].

In the case of the Ge 580 °C sample, the Ge concentration versus depth profiles was measured by secondary ion mass spectrometry (SIMS) with a Cameca IMS 7f microanalyzer (the Ge detection limit was estimated in $\sim 5 \times 10^{16}$ cm^{-3}). A 10 keV O^{2+} primary beam with a current of 600 nA was rastered over a 150 × 150 μm^2 area and secondary ions were collected from the central part of the sputtered crater. The intensity-concentration calibration was performed using Ge-ion-implanted samples as a reference. The conversion from sputtering time to sample depth was performed by

measurement of the crater depth using a Dektak 8 stylus profilometer and assuming a constant erosion rate.

The results of SIMS measurements are shown in Fig. 1(b) in a logarithmic scale as a function of the milled depth. A large Ge concentration is found in both the GaAs buffer and $Al_{0.3}Ga_{0.7}As$ layer, denoting a Ge diffusion from the substrate into the molecular-beam-epitaxy-grown layers. Here the Ge contamination reaches the value of $\rho_{Ge} \simeq 10^{17}\,cm^{-3}$ (not very different from the values reported in Refs. [69,70] for similar samples), sufficiently large to form an impurity band. Indeed, according to the Mott criterion for GaAs, the critical doping n_c to form a band (defined as $a_B n_c^{1/3} = 0.25$, where a_B is the Bohr radius) is $n_c \simeq 1.3 \times 10^{16}\,cm^{-3}$ [53]. The relatively large Ge contamination of the $Al_{0.3}Ga_{0.7}As$ alloy is an important clue for the attribution of extrinsic quantum emitters to Ge centers, which will be discussed in the following. The large increase of the Ge content near the surface [first 50 nm; see Fig. 1(b)] is likely due to segregation of Ge on the GaAs surface during the growth and/or Ge out-diffusion towards the surface.

III. NATURE OF THE DEFECTS AND ENSEMBLE SPECTRA

Before addressing the optical properties of the extrinsic quantum emitters in $Al_{0.3}Ga_{0.7}As$, we unambiguously validate their origin as due to Ge centers by comparing the emission of purely III-V samples with that of those grown on silicon and germanium. This is also done in order to exclude the presence of Al-poor clusters in the $Al_xGa_{1-x}As$ matrix. In fact, the presence of such Al-poor zones has been recently proposed [71,72] as a possible explanation of bright and sharp PL lines (emitting from $\sim$1.7 eV up to $\sim$2 eV) in $Al_xGa_{1-x}As$ nanowires [67,68]. Note that the excitonic emission from those clusters [71,72] falls in a similar spectral interval of the Ge-defects emission investigated here (emitting from $\sim$1.8 eV up to $\sim$1.87 eV).

In order to promote some alloy disorder, possibly producing Al-poor nanoclusters within the $Al_{0.3}Ga_{0.7}As$ layer, we grew the two reference samples GaAs 400 °C and GaAs 580 °C. The micro-PL spectra at low temperature (10 K) of the two test samples are compared with the $Al_{0.3}Ga_{0.7}As$ layer grown on Ge substrate in Fig. 2. One-dimensional (1D) maps (energy vs space), with the detected PL intensity represented as a false-color scale, are shown for each of the three samples. The top panels of Figs. 2(a)–2(c) display the full scan (100 μm long) while the bottom panels show a typical spectrum collected in a single point. In all three samples we can identify the bound exciton emission (Bex) and the usual band from shallow centers due to carbon-related residual contamination (DA-C) [73,74]. This latter band is usually present in AlGaAs layers grown by molecular beam epitaxy [73–76]. By comparing the Bex and DA-C PL bands in the three spectra, we conclude that the Al content is about 5% larger in the GaAs 400 °C sample with respect to the 580 °C sample. At the same time the Al content of the Ge 580 °C sample is slightly larger (of the order of 1%) than the GaAs 580 °C sample. Apart from these unintentional differences in the calibration of the $Al_xGa_{1-x}As$ alloy, we note a relevant structuring of the DA-C band with sharp lines spatially localized, together with an overall reduced emission efficiency for the lower growth temperature and a broader extension of the DA-C band when compared with a similar sample grown at 650 °C (not shown).

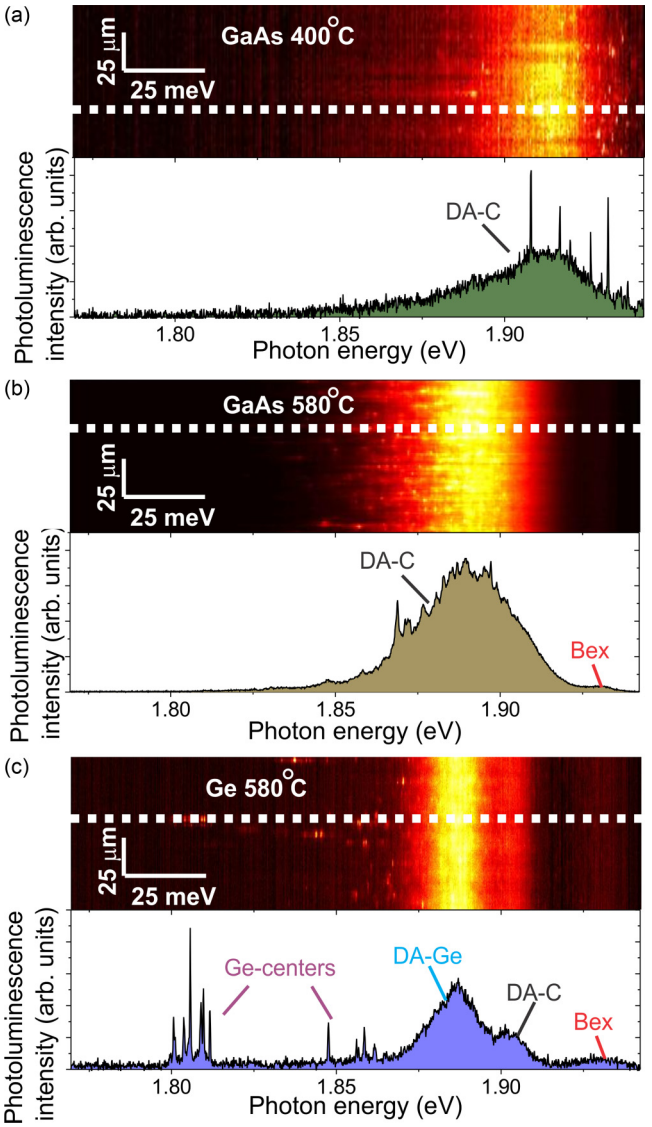

FIG. 2. (Color online) (a)–(c) Top panel shows a 1D scan over 100 μm (in 0.5 μm steps) on samples GaAs 400 °C, GaAs 580 °C, and Ge 580 °C. The white dashed line highlights the spatial position of the spectrum shown in the corresponding bottom panel. Bottom panels: Typical PL spectrum extracted from the 1D scan in the top panel.

Quite peculiar is the PL spectrum of the sample grown on a Ge substrate where, besides the presence of the same PL structures (DA-C band and Bex band), we observe two other contributions at lower energy [see Fig. 2(c) and previously reported data in Refs. [67,68]]. These two new PL contributions appear as a broad PL band at $\sim$1.88 eV together with, at lower energies, a tail extending until $\sim$1.80 eV where several sharp, isolated and bright lines organized in *multiplets* are found. Due to the relevant Ge contamination determined by the SIMS measurements reported in Fig. 1(b), the broadband at around $\sim$1.88 eV is ascribed to Ge-related donor-acceptor recombination (it will be denoted as DA-Ge band in the following) [73–76]. Similarly to the case of the DA-C band,

also the DA-Ge band may show sharp and spatially localized lines. Finally and accordingly with the previous literature, the tail extending to lower energy is interpreted as emission from deep donor-acceptor levels [47,77–79].

In two recent papers, we showed that the sharp lines emissions below the DA-Ge band show antibunching and biexciton recombination [67,68]. The comparison with Ge-free samples and the data from SIMS measurements, demonstrate that the Al-poor nanoclusters, leading to natural QDs in the $Al_xGa_{1-x}As$ alloy (as observed in Refs. [71,72]), do not play a role in the attribution of the sharp lines organized in localized multiplets which are observed only in the sample grown on the Ge substrate. This new finding leads us to conclude that the extrinsic centers under investigation have to be ascribed to the presence of Ge contamination in the $Al_{0.3}Ga_{0.7}As$ layer.

We now focus our attention on the case of the sample grown on a germanium substrate by performing extended two-dimensional (2D) PL maps at low excitation power. In Fig. 3(a) we highlight three spectral intervals: I for Ge-impurities emission, II for the DA-Ge and DA-C emission, and zone III for the Bex emission. In Fig. 3(b) are displayed the results of a surface scan spectrally integrated over the three intervals highlighted in Fig. 3(a). We observe a strong spatial localization of the emitted intensity from the spectral interval I [Fig. 3(b), left panel] in bright spots which lateral extension in space reflects our instrumental resolution. For the zones II and III instead [Fig. 3(b), central and right panels, respectively], a rather uniform intensity distribution is observed (see also the maps reported in the Supplemental Material [80,81]). The dark area in the top-right part of the images is attributed to an extended defect of the crystal or to some impurity on the sample surface.

The micro-PL mapping allows for a precise counting of the emitting Ge impurities within the investigated sample surface (and sample thickness). Integrating over two maps of $50 \times 50\,\mu m^2$ we find a surface density of spatially localized and sharp peaks of $\sim 2.5 \times 10^{-2}\ \mu m^{-2}$. By taking into account the thickness of the $Al_{0.3}Ga_{0.7}As$ layer, we evaluate a concentration of $\rho_{PL} \simeq 10^{11}\,cm^{-3}$ which is by far smaller than the concentration of Ge ions measured in SIMS $\rho_{Ge} \sim 10^{17}\,cm^{-3}$ [see Fig. 1(b)].

The low density of quantum emitters and their PL spectra with multiple lines is an indication of the complex nature of these extrinsic centers. As for similar systems of extrinsic centers able to accommodate multiexcitonic states [51–55], we believe that a likely attribution of the defects responsible for the isolated emission below 1.87 eV can be the presence of binary systems or more generally, complex defects. As an example, let us explicitly refer to the attribution of N dyads in AlAs as responsible for biexciton emission [55] and tentatively assume that our extrinsic centers were related to pairs of Ge impurities. With this hypothesis and assuming a stochastic model [45,55] it is possible to compare the measured density of emitting centers (ρ_{PL}) with that of pairs of Ge ions ($\rho_{Ge\text{-}Ge} = \rho_{Ge}^2 V$ where $V = d_{Ge\text{-}Ge}^3$ is the volume occupied by a pair). We can roughly estimate the typical distance between two ions $d_{Ge\text{-}Ge}$ in the ~ 0.1 nm range which well compares with the lattice constant of the host semiconductor matrix. This estimate strongly supports the idea of extrinsic centers related to Ge pairs, even if a different hypothesis cannot be ruled out at the moment. Then in the following we will refer to them as Ge-centers emission.

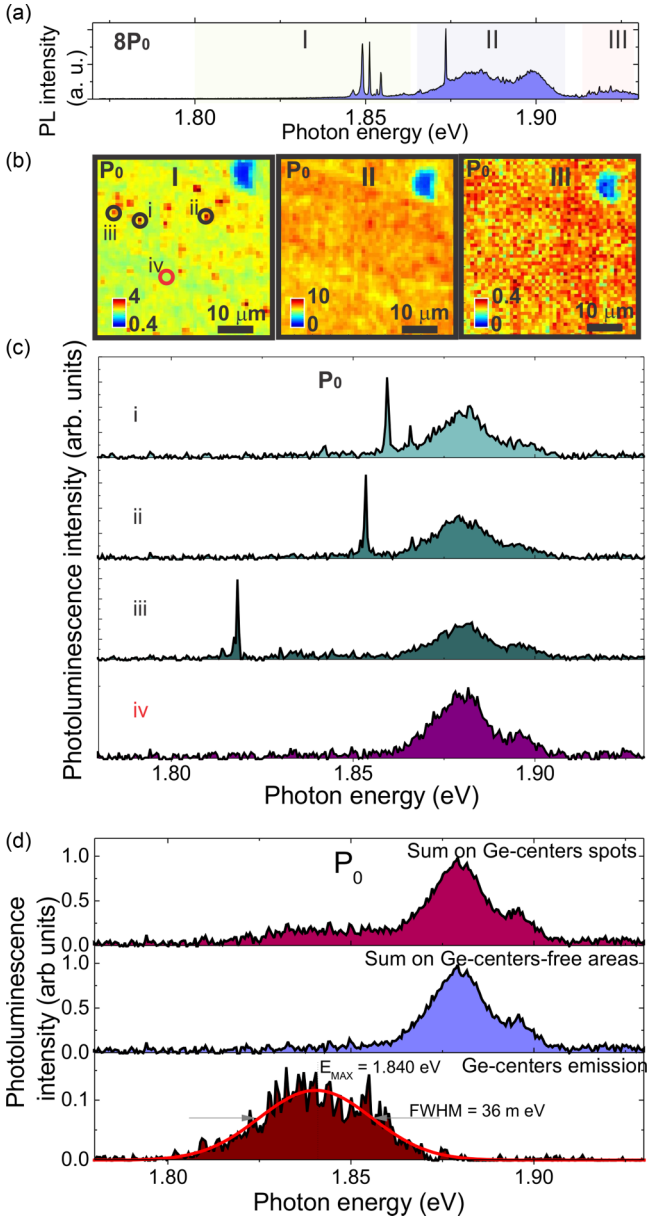

FIG. 3. (Color online) (a) Typical PL spectrum from the sample Ge 580 °C. The shaded areas I, II, and III highlight the spectral intervals used to represent the spectral map shown in (b). (b) $50 \times 50\,\mu m^2$ spectral map integrated on the three different spectral intervals I, II, and III highlighted in (a). The excitation power density was $P_0 = 5 \times 10^2\ W/cm^2$. Similar maps but with a sharper spectral filtering are shown as an animated map in the Supplemental Material [80,81]. In the left panel I four spots (i, ii, iii, and iv) are highlighted and the corresponding extracted spectra are shown in (c). (d) Top panel: Integrated and normalized emission from Ge centers. Central panel: Same as top panel but for Ge-centers-free areas (i.e., "bulk" $Al_{0.3}Ga_{0.7}As$). Bottom panel: Isolated Ge-centers emission obtained as intensity difference between the two spectra in the top and middle panels. The continuous red line is a Gaussian fit to the data.

Finally, we remark that this hyperspectral imaging technique [82] allows the detection of complex dopant

impurities [66] with an extremely high sensitivity (note that the most accurate SIMS measurements can reach $\sim 10^{13}$ cm^{-3}). Differently from conventional near-field microscopy techniques for doping detection [46], we can gather additional information about the energy of each defect within the energy band gap of the host material and thus, *a posteriori*, we can rebuild the full spectrum of the Ge centers [see Fig. 3(d)].

Combining the spectral information with the mapping over large areas of the sample, a precise characterization of the ensemble emission can be extracted despite the very low density of the Ge centers. As a matter of fact, standard macro-PL measurements do not allow one to extract the spectral emission band of these Ge centers [67]. The basic idea is to sum up only the micro-PL spectra arising from points containing the Ge-centers emission. This means that within the two $50 \times 50\,\mu$m^2 spectral maps, containing 2500 different points each, we operate a careful selection of 150 micro-PL spectra corresponding to individual Ge-centers emission. In this way we can build *a posteriori* a *pseudo-macro-PL* spectrum by summing them and normalizing the total spectrum to its maximum intensity.

The result of this operation is shown in the top panel (*Sum on Ge-centers spots*) of Fig. 3(d). The same procedure is applied to micro-PL spectra where no localized and sharp emission is present (*Sum on Ge-centers-free areas*), thus recovering the "bulk"-like emission of $Al_{0.3}Ga_{0.7}As$. This is shown in the central panel of Fig. 3(d). Clearly the emission of the sharp lines is perfectly rejected in these spectra where only DA-Ge, DA-C, and Bex are visible.

The large broadening of the PL band of the Ge centers may reflect either random distribution of the ion-to-ion distance $d_{\text{Ge-Ge}}$ of the Ge centers in the host material or the spectral diffusion associated with stochastic variations of the electric field [83–92] and/or alloy around the Ge centers. The large broadening is also in stark contrast with what is found in other systems such as carbon [62,63] and copper [64,65] impurities in silicon or nitrogen pairs in AlAs or GaAs [50,55,93], featuring a well-defined emission energy reflecting a limited number of optically active configurations for the impurities while it looks similar to what was found in Te dyads in ZnSe [50,93,94], Mn in ZnS [95], and carbon-antisite pairs in SiC [66] where a relevant spread in the emission energy is present. At the same time, this large variation of excitonic recombination can be an advantage if a tuning or a selection of peculiar emission properties is needed. Note also that the emission of Ge centers is related to the band gap of the host alloy, and then, in principle, a control of the emission energy could be obtained by tuning the Al content or preliminarily using different III-V alloys. This is important for controlling the emission of these quantum sources to specific targets [8,9] or for coupling them to other optical devices (such as optical fibers or resonators).

IV. MULTIEXCITON EMISSION

As found for other complex defects [93,94] the Ge centers in study support charged excitons and multiexciton features. We note that, considering a statistical analysis of $\sim$150 Ge centers, practically all of them (more than 90%) show these features and we thus conclude that the Ge centers in study support all the energy states typical of s-shell recombination: up to two bound electrons and two holes (in conduction and valence bands, respectively). A preliminary assignment of neutral exciton, biexciton, and charged exciton was previously done by power dependence and fine structure splitting measurements [67,68]. Here we complete the full picture of the electronic states of the s shell addressing both the positive (X^+) and negative (X^-) charged exciton levels. At the same time, we evaluate the capture volume and the carrier localization through the analysis of the saturation power [96].

In Fig. 4(a) we show typical PL spectra of an individual Ge center at different power densities. The emission clearly shows additional spectral components ascribed to biexcitons and charged exciton complexes [68]. The corresponding evolution of the PL intensities with power is displayed in Fig. 4(b). Here, according to a Poissonian model for the level occupation probability [96] the three main PL lines follow slightly different filling dynamics [the fits shown in Fig. 4(b) correspond to $I_{PL} \propto (\alpha \mathcal{P}^{\beta})^m \exp[-(\alpha \mathcal{P}^{\beta})^m]$ where $m = 1,1.5,2$ corresponds, respectively, to one exciton (X), one exciton plus a spectator charge ($X^{\pm}$), and two excitons (XX); $\mathcal{P}$ is the excitation power; α and β are fitting parameters describing the capture mechanism and their corresponding values extracted from the fit are directly reported in Fig. 4(b)]. The dependence on the excitation power [96], the line broadening [86], and the relative spectral position [97] leads us to the attribution of the lines to X^-, XX, and X. The X line reported in Fig. 4(b) shows a saturation power of about $\mathcal{P}_{\text{sat}} \simeq 0.6$ mW, while slightly different values (not shown) were observed for other Ge-centers (from $\sim$0.05 up to $\sim$1 mW). This feature possibly reflects a different capture efficiency due to the presence of extrinsic effects related to disorder in the electrostatic environment of the emitters [88,90–92,96,98].

The saturation power of X (i.e., the value $\mathcal{P}_{\text{sat}}$ for the maximum occupation probability) allows one to estimate the capture length of the Ge centers [96]. From the typical values of $\mathcal{P}_{\text{sat}}$ for X and taking into account the experimental conditions, we estimate a capture length ranging from $\sim$30 nm up to $\sim$10 nm, similar to or smaller than that found for $GaAs/Al_{0.3}Ga_{0.7}As$ epitaxial quantum dots [96,99,100] investigated with the same experimental apparatus and with similar excitation conditions.

Clear-cut attribution of the exciton-biexciton cascade and charged exciton comes from fine structure splitting measurements: An example of a different individual Ge center showing X^+, XX, and X is reported in Fig. 4(c). The X and XX lines shift symmetrically when changing the detected polarization angle, while the X^+ line does not shift [37,43,86,96].

Let us now consider the line broadening of the different recombination lines as an additional key for attributing the excitonic complexes [see Fig. 4(d)]. From a statistical point of view we observe a wide spread of values of the linewidth ranging from few tens up to few hundreds of μeV; still the order from the sharper to the broader lines among the different excitonic complexes does not vary: $\sigma_{X^-} \sim \sigma_X > \sigma_{X^+} > \sigma_{XX}$ (for the sake of thoroughness we note that X^- featuring larger or smaller broadening with respect to the corresponding X can be found). The Gaussian broadening of the low temperature PL emission of individual excitonic transitions is commonly ascribed to spectral diffusion

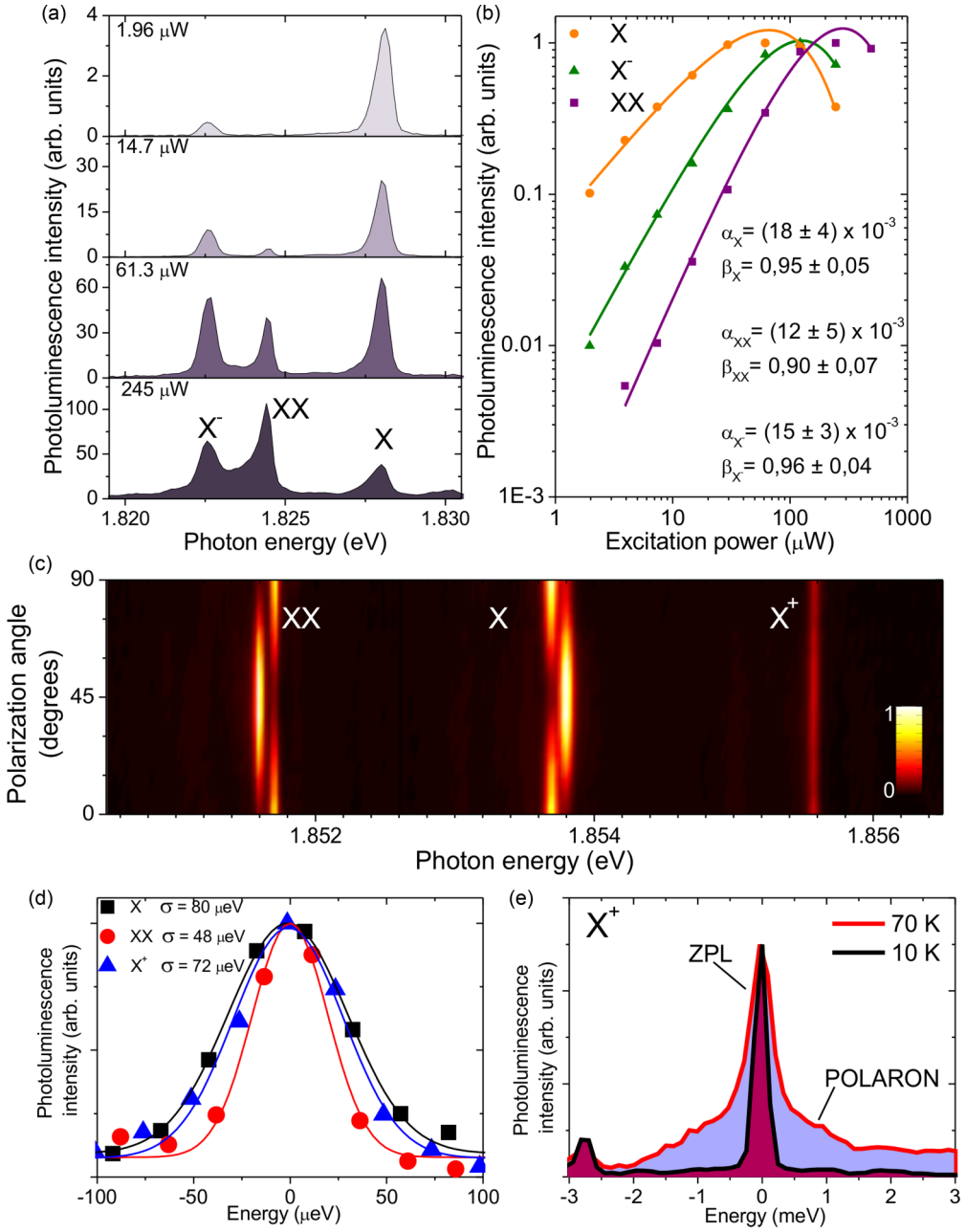

FIG. 4. (Color online) (a) Series of PL spectra at different excitation power of an individual Ge impurity exhibiting X^-, XX, and X recombination. (b) Summary of the PL intensity as a function of the excitation power $\mathcal{P}$ of the data reported in (a). Symbols are the experimental data while the lines represent Poissonian fit. (c) Polarization map of an individual Ge impurity exhibiting XX, X, and X^+ recombination. (d) X, XX, and X^+ normalized and energy-shifted emission at 10 K. The continuous lines are Gaussian fit to the data. (e) Normalized spectra of X^+ emission at 10 and 70 K. The zero-phonon-line (ZPL) and the polaron emission are highlighted.

[83–92] and a hierarchical broadening (showing $\sigma_{X^-} \sim \sigma_X > \sigma_{X^+} \sim \sigma_{XX}$) has been already found in epitaxial quantum dots [86,87,101,102] and impurities [72]. This behavior can be explained in terms of a *selective* quantum-confined Stark effect induced by the presence of charged defects in the semiconductor matrix [86,87]. The relative position of the charged trap results in a different Stark shift amplitude (and eventually sign) for each excitonic complex. On one hand, the analogy with QDs is expected for any strongly confining potential able to localize the electrons and holes at the nanometer scale, as in the case of the Ge centers in study. On the other hand, we did use this analogy with QDs in order to attribute the emission lines to different excitonic complexes. In this respect the hierarchical broadening is a confirmation of the soundness of our attribution.

In view of possible integration in optoelectronic devices it is also needed to increase the operation temperature of the quantum sources as much as possible. Indeed we were able to follow the emission of the Ge centers up to 70 K. Following the temperature-induced redshift of any excitonic recombination, we observe an initial linear decrease in energy and then a steeper quadratic decrease (as reasonably expected for

electronic transitions in semiconducting materials according to the Varshni empirical law of AlGaAs alloy) [103,104]. While at low temperature only a sharp line is visible, with a spectral broadening limited by our low resolution (in these data) at higher temperature we assist to a slight broadening of the central sharp line together with the onset of a broad pedestal [84,105–109]. These features can be interpreted in terms of electron-acoustic phonon interaction: In analogy with epitaxial quantum dots, we assign the sharp component of the single Ge-impurities emission to the exciton zero phonon line [ZPL in Fig. 4(e)], while the sidebands to a superposition of acoustic phonon replicas. The still sharp emission at $T = 70$ K and the limited thermal quenching of the PL (quite similar to what is observed in GaAs QDs) lead us to state the possibility to use the Ge centers as quantum emitters at liquid nitrogen temperature.

V. BINDING ENERGY OF XX, X^+, AND X^-

We now address the issue of the Coulombic interactions between electrons and holes trapped by Ge impurities which are responsible for the lifted degeneracy of the neutral exciton state as well as for the energy renormalization of the electronic states within individual impurity centers.

Due to asymmetries in the confinement potential and local strain accumulation the two spin states of the bright neutral exciton are split by the so-called fine structure splitting (FSS) associated with the exchange interaction [26,35–37,43,55,110]; for the Ge centers in study, it has been shown that the FSS is in the $\sim$100 μeV range [see Fig. 4(c)] [68].

The so-called exciton binding energy is simply defined as the energy shift with respect to the corresponding neutral exciton line ($BE_{XX} = E_X - E_{XX}$). Similarly, one can define the charged exciton binding energy as $BE_{X^\pm} = E_X - E_{X^\pm}$. The binding energy arises from the complicated interplay of direct Coulombic interactions, exchange and correlation typical of each excitonic species [37,42,44,93,97,111–115].

Generally speaking three scenarios can occur: the binding energy is positive, zero, or negative. In the case of the biexciton complex these cases are represented in Fig. 5(a) also including the presence of FSS (not in scale). In the left panel of Fig. 5(a) is displayed the situation of a XX having positive binding energy $BE_{XX} > 0$. In this condition (if FSS $\neq 0$) the emitted photons in the biexciton cascade are discernible in energy and polarization. If instead the FSS vanishes, the XX and X photons are polarization entangled [4,15,20,25–28,34,38]. In the central panel of Fig. 5(a) is shown a XX with a zero binding energy $BE_{XX} = 0$ where the emission energy of H-(V) polarized XX photons matches that of the V-(H) polarized X photon. The two photons are not distinguishable in energy and thus polarization entanglement can be recovered with a time-reordering scheme [39,40]. Finally, in the right panel, it is shown the case of negative binding energy ($BE_{XX} < 0$); here the same considerations made for the left panel apply. Therefore, in view of realizing a quantum source of entangled photon pairs, the condition can be FSS $= 0$ or $BE_{XX} = 0$.

Let us now consider the experimental data for the binding energies of the excitonic complex localized at the Ge centers. As most of these transitions were mainly attributed through

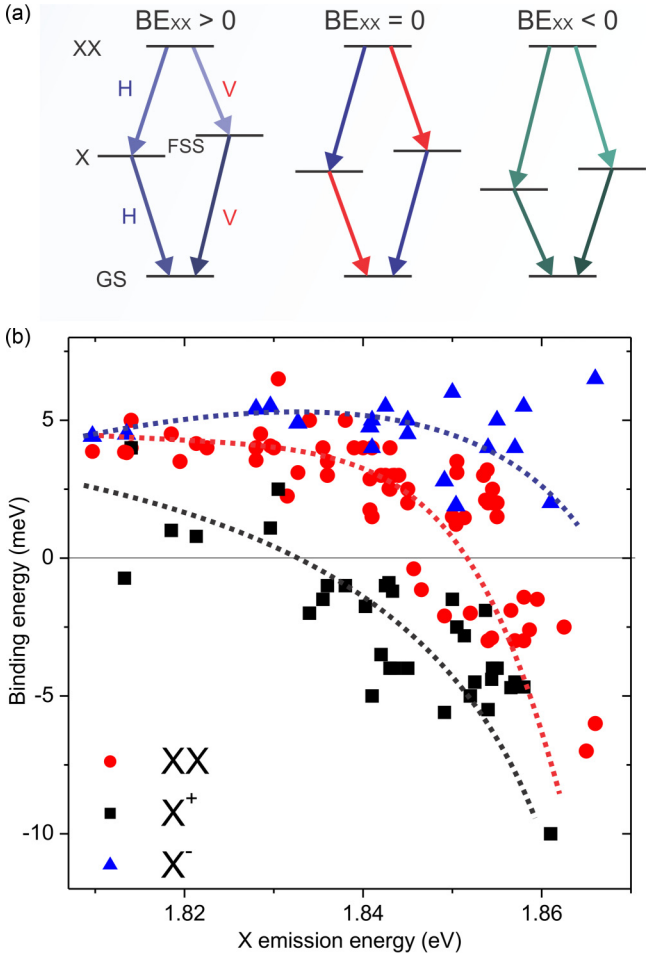

FIG. 5. (Color online) (a) Scheme of X and XX energy levels for three different binding energies of XX; from left to right: positive, zero, and negative. V and H highlight the linear polarization of the emitted photons. (b) Binding energy of X^-, X^+, and XX. Dotted lines are guides to the eyes.

their power dependence it is usually easy to have a clear attribution of X and XX while the X^+ and X^- attributions are sometimes less certain. Disregarding the ambiguous cases leads to a lower statistic for X^+ and X^-. A summary of the data with excitonic recombination ranging from $\sim$1.81 eV to $\sim$1.86 eV is given in Fig. 5(b). Pronounced features emerging from this analysis are summarized as follows:

(1) The binding energy of X^+ shows a decreasing trend when increasing X emission energy from $\sim+1$ meV to ~-5 meV, with a transition from binding to antibinding.

(2) The XX state shows a binding energy of $\sim+4$ meV at low energy and abruptly evolves toward negative values above 1.855 eV reaching the negative value of ~-6 meV with a steep trend.

(3) The binding energy of X^- is always positive ($BE_{X^-} \simeq$ 5 meV), thus X^- forms a bound state. Its evolution with the three-dimensional (3D) confinement is quite constant even if the number of points is quite small due to the problematic attribution of this line.

Differently from bulk semiconductors where the physics of excitons is determined by correlation effects, in strongly

confining systems (i.e., quantum wells and quantum dots) where the size of the potential for electrons and holes approaches the bulk excitonic Bohr radius ($\sim$11 nm in GaAs compounds) the direct electron-hole Coulomb interactions dominate over the correlation term. In this case the many-body problem for the charged excitons and biexciton binding energy can be approximated by considering the sum of the interactions between all the pairs of particles composing the excitonic complex [44,111,112,116]. This scheme is similar to the Hartree mean-field correction method where each element of the system is considered in interaction with the mean field produced by all the other particles that are present.

Comparing the present results for the binding energy of Ge impurities with calculations and experimental data for quantum dots or monolayer fluctuation of quantum wells [97,112–115,117] we can see a remarkable agreement with the behavior predicted and measured for a truly 3D confinement [97,112] (i.e., a small quantum dot without a wetting layer). XX and X^+ show a steep reduction in the binding energy and eventually a change of its sign, while X^- is always positive. This suggests the presence of an attractive exciton-electron potential (for the X^-), while the negative binding energy of XX and X^+ accounts for an overall repulsive exciton-exciton and exciton-hole potential (for the XX and X^+, respectively).

This behavior is qualitatively explained by the different confinements of electron and hole wave functions which, in turn, are ruled by their different effective masses [97,112]: The *heavier* hole is more localized at the center of the potential with respect to the electron (note that for $Al_{0.3}Ga_{0.7}As$ the ratio of electron and heavy-hole effective mass is $m_e^*/m_{hh}^* \simeq 0.15$). As a consequence, in the presence of a bound electron-hole pair, the larger positive carrier density at the center of the confining potential leads to an attractive Coulomb potential for an electron and a repulsive one for a hole. The same considerations hold for the case of two bound excitons.

These findings are in contrast with common epitaxial quantum dots with a weaker lateral confinement originated by a 2D wetting layer: In these cases a linear dependence of the XX and X^+ binding energy as a function of the X emission is usually found together with a dominantly binding nature of the XX state [42,44,97,115,117].

We conclude that a strong carrier localization is present for high-energy Ge centers, while the positive values of the binding energy found at lower X emission energy suggests a recovered dominant effect of the correlation term. Most importantly, a XX state emitting at energies close to that of the corresponding X state can be achieved, thus allowing for an easier implementation of a time-reordering scheme for entangled photons [39,40] eventually with the help of a (small) external field for the fine tuning [25,28,34].

VI. CONCLUSIONS

In conclusion we have shown that the single-photon emitters recently reported [67,68] are related to Ge centers and come from unintentional contamination of the III-V layers grown on germanium substrates. These centers provide a valuable alternative to epitaxial quantum dots for the implementation of different carrier states such as X, XX, X^+, and X^- and, in analogy with similar impurities, could be in principle implemented through ionic implantation [60,62–66]. Due to the strong carrier confinement the Ge centers feature similar properties to the epitaxial quantum dot counterpart, present a line broadening dominated by a quantum-confined Stark effect at low temperature, and a phonon coupling at higher temperatures. The optical properties of the excitonic recombination from Ge centers are quite good: a linewidth as sharp as 40 μeV can be found at high excitation power densities and low temperature; the emission is still bright at 70 K, confirming the good thermal stability of this class of emitters. The electronic states populating the s shell well agree with what is found for a fully 3D confining potential in quantum dots and thus enable the implementation of quasidegenerate X and XX states.

Our findings suggest the use of the PL emission of Ge extrinsic centers in $Al_{0.3}Ga_{0.7}As$ as a versatile platform for obtaining single photons on a large spectral range and entangled photons based on the time reordering scheme [39,40], for spin-photon turnstile devices and for slow light when coupled with atomic vapors [8,9]. We stress that, differently from most III-V compounds where Stranski-Krastanov quantum dots are obtained, the emission of these Ge centers well matches the highest detection efficiency of Si-based single-photon detectors ensuring a high fidelity in the detection and not only in the preparation of the quantum state of the system [14]. Last but not least, these results have been obtained on silicon and germanium substrates opening up new avenues for the exploitation of quantum emitters within a device-friendly platform.

ACKNOWLEDGMENTS

This work has been carried out thanks to the support of the European project LASERLAB-EUROPE (Grant Agreement No. 284464, EC's Seventh Framework).

[1] A. Imamoğlu, D. D. Awschalom, G. Burkard, D. P. DiVincenzo, D. Loss, M. Sherwin, and A. Small, Quantum information processing using quantum dot spins and cavity QED, Phys. Rev. Lett. **83**, 4204 (1999).

[2] C. H. Bennett, Quantum information and computation, Phys. Today **48**(10), 24 (2008).

[3] M. A. Nielsen and I. L. Chuang, *Quantum Computation and Quantum Information* (Cambridge University Press, Cambridge, England, 2010).

[4] X. Li, Y. Wu, D. Steel, D. Gammon, T. Stievater, D. Katzer, D. Park, C. Piermarocchi, and L. Sham, An all-optical quantum gate in a semiconductor quantum dot, Science **301**, 809 (2003).

[5] D. Fattal, E. Diamanti, K. Inoue, and Y. Yamamoto, Quantum teleportation with a quantum dot single photon source, Phys. Rev. Lett. **92**, 037904 (2004).

[6] A. Politi, J. C. Matthews, and J. L. O'Brien, Shors quantum factoring algorithm on a photonic chip, Science **325**, 1221 (2009).

[7] F. Troiani, U. Hohenester, and E. Molinari, Exploiting exciton-exciton interactions in semiconductor quantum dots for quantum-information processing, Phys. Rev. B **62**, R2263 (2000).

[8] N. Akopian, L. Wang, A. Rastelli, O. Schmidt, and V. Zwiller, Hybrid semiconductor-atomic interface: Slowing down single photons from a quantum dot, Nat. Photonics **5**, 230 (2011).

[9] P. Siyushev, G. Stein, J. Wrachtrup, and I. Gerhardt, Molecular photons interfaced with alkali atoms, Nature (London) **509**, 66 (2014).

[10] K. De Greve, L. Yu, P. L. McMahon, J. S. Pelc, C. M. Natarajan, N. Y. Kim, E. Abe, S. Maier, C. Schneider, M. Kamp *et al.*, Quantum-dot spin-photon entanglement via frequency downconversion to telecom wavelength, Nature (London) **491**, 421 (2012).

[11] W. Gao, P. Fallahi, E. Togan, J. Miguel-Sanchez, and A. Imamoglu, Observation of entanglement between a quantum dot spin and a single photon, Nature (London) **491**, 426 (2012).

[12] R. J. Warburton, Single spins in self-assembled quantum dots, Nat. Mater. **12**, 483 (2013).

[13] B. Lounis and M. Orrit, Single-photon sources, Rep. Prog. Phys. **68**, 1129 (2005).

[14] M. Eisaman, J. Fan, A. Migdall, and S. Polyakov, Invited review article: Single-photon sources and detectors, Rev. Sci. Instrum. **82**, 071101 (2011).

[15] G. Chen, N. Bonadeo, D. Steel, D. Gammon, D. Katzer, D. Park, and L. Sham, Optically induced entanglement of excitons in a single quantum dot, Science **289**, 1906 (2000).

[16] V. Zwiller, H. Blom, P. Jonsson, N. Panev, S. Jeppesen, T. Tsegaye, E. Goobar, M.-E. Pistol, L. Samuelson, and G. Björk, Single quantum dots emit single photons at a time: Antibunching experiments, Appl. Phys. Lett. **78**, 2476 (2001).

[17] D. V. Regelman, U. Mizrahi, D. Gershoni, E. Ehrenfreund, W. Schoenfeld, and P. M. Petroff, Semiconductor quantum dot: A quantum light source of multicolor photons with tunable statistics, Phys. Rev. Lett. **87**, 257401 (2001).

[18] T. H. Stievater, X. Li, D. G. Steel, D. Gammon, D. S. Katzer, D. Park, C. Piermarocchi, and L. J. Sham, Rabi oscillations of excitons in single quantum dots, Phys. Rev. Lett. **87**, 133603 (2001).

[19] X. Brokmann, G. Messin, P. Desbiolles, E. Giacobino, M. Dahan, and J. Hermier, Colloidal CdSe/ZnS quantum dots as single-photon sources, New J. Phys. **6**, 99 (2004).

[20] R. M. Stevenson, R. J. Young, P. Atkinson, K. Cooper, D. A. Ritchie, and A. J. Shields, A semiconductor source of triggered entangled photon pairs, Nature (London) **439**, 179 (2006).

[21] H. Kumano, S. Kimura, M. Endo, H. Sasakura, S. Adachi, S. Muto, and I. Suemune, Deterministic single-photon and polarization-correlated photon pair generations from a single InAlAs quantum dot, J. Nanoelectron. Optoelectron. **1**, 39 (2006).

[22] M. Abbarchi, C. A. Mastrandrea, A. Vinattieri, S. Sanguinetti, T. Mano, T. Kuroda, N. Koguchi, K. Sakoda, and M. Gurioli, Photon antibunching in double quantum ring structures, Phys. Rev. B **79**, 085308 (2009).

[23] T. Kuroda, T. Belhadj, M. Abbarchi, C. Mastrandrea, M. Gurioli, T. Mano, N. Ikeda, Y. Sugimoto, K. Asakawa, N. Koguchi *et al.*, Bunching visibility for correlated photons from single GaAs quantum dots, Phys. Rev. B **79**, 035330 (2009).

[24] A. Ulhaq, S. Weiler, S. Ulrich, R. Roßbach, M. Jetter, and P. Michler, Cascaded single-photon emission from the Mollow triplet sidebands of a quantum dot, Nat. Photon. **6**, 238 (2012).

[25] R. Trotta, P. Atkinson, J. Plumhof, E. Zallo, R. Rezaev, S. Kumar, S. Baunack, J. Schroeter, A. Rastelli, and O. Schmidt, Nanomembrane quantum-light-emitting diodes integrated onto piezoelectric actuators, Adv. Mater. **24**, 2668 (2012).

[26] T. Kuroda, T. Mano, N. Ha, H. Nakajima, H. Kumano, B. Urbaszek, M. Jo, M. Abbarchi, Y. Sakuma, K. Sakoda *et al.*, Symmetric quantum dots as efficient sources of highly entangled photons: Violation of Bell's inequality without spectral and temporal filtering, Phys. Rev. B **88**, 041306 (2013).

[27] H. Jayakumar, A. Predojević, T. Huber, T. Kauten, G. S. Solomon, and G. Weihs, Deterministic photon pairs and coherent optical control of a single quantum dot, Phys. Rev. Lett. **110**, 135505 (2013).

[28] R. Trotta, J. S. Wildmann, E. Zallo, O. G. Schmidt, and A. Rastelli, Highly entangled photons from hybrid piezoelectric-semiconductor quantum dot devices, Nano Lett. **14**, 3439 (2014).

[29] S. Birindelli, M. Felici, J. S. Wildmann, A. Polimeni, M. Capizzi, A. Gerardino, S. Rubini, F. Martelli, A. Rastelli, and R. Trotta, Single photons on demand from novel site-controlled GaAsN/GaAsN:H quantum dots, Nano Lett. **14**, 1275 (2014).

[30] A. Högele, C. Galland, M. Winger, and A. Imamoğlu, Photon antibunching in the photoluminescence spectra of a single carbon nanotube, Phys. Rev. Lett. **100**, 217401 (2008).

[31] T. Basché, W. E. Moerner, M. Orrit, and H. Talon, Photon antibunching in the fluorescence of a single dye molecule trapped in a solid, Phys. Rev. Lett. **69**, 1516 (1992).

[32] C. Brunel, B. Lounis, P. Tamarat, and M. Orrit, Triggered source of single photons based on controlled single molecule fluorescence, Phys. Rev. Lett. **83**, 2722 (1999).

[33] B. Lounis and W. Moerner, Single photons on demand from a single molecule at room temperature, Nature (London) **407**, 491 (2000).

[34] R. Trotta, E. Zallo, C. Ortix, P. Atkinson, J. D. Plumhof, J. van den Brink, A. Rastelli, and O. G. Schmidt, Universal recovery of the energy-level degeneracy of bright excitons in InGaAs quantum dots without a structure symmetry, Phys. Rev. Lett. **109**, 147401 (2012).

[35] T. Mano, M. Abbarchi, T. Kuroda, B. McSkimming, A. Ohtake, K. Mitsuishi, and K. Sakoda, Self-assembly of symmetric GaAs quantum dots on (111)A substrates: Suppression of fine-structure splitting, Appl. Phys. Express **3**, 065203 (2010).

[36] N. Ha, X. Liu, T. Mano, T. Kuroda, K. Mitsuishi, A. Castellano, S. Sanguinetti, T. Noda, Y. Sakuma, and K. Sakoda, Droplet epitaxial growth of highly symmetric quantum dots emitting at telecommunication wavelengths on InP (111)A, Appl. Phys. Lett. **104**, 143106 (2014).

[37] X. Liu, N. Ha, H. Nakajima, T. Mano, T. Kuroda, B. Urbaszek, H. Kumano, I. Suemune, Y. Sakuma, and K. Sakoda, Vanishing fine-structure splittings in telecommunication-wavelength quantum dots grown on (111)A surfaces by droplet epitaxy, Phys. Rev. B **90**, 081301 (2014).

[38] N. Akopian, N. H. Lindner, E. Poem, Y. Berlatzky, J. Avron, D. Gershoni, B. D. Gerardot, and P. M. Petroff, Entangled photon

pairs from semiconductor quantum dots, Phys. Rev. Lett. **96**, 130501 (2006).
[39] F. Troiani and C. Tejedor, Entangled photon pairs from a quantum-dot cascade decay: The effect of time reordering, Phys. Rev. B **78**, 155305 (2008).
[40] J. E. Avron, G. Bisker, D. Gershoni, N. H. Lindner, E. A. Meirom, and R. J. Warburton, Entanglement on demand through time reordering, Phys. Rev. Lett. **100**, 120501 (2008).
[41] S. Rodt, R. Heitz, A. Schliwa, R. L. Sellin, F. Guffarth, and D. Bimberg, Repulsive exciton-exciton interaction in quantum dots, Phys. Rev. B **68**, 035331 (2003).
[42] S. Rodt, A. Schliwa, K. Pötschke, F. Guffarth, and D. Bimberg, Correlation of structural and few-particle properties of self-organized InAs/GaAs quantum dots, Phys. Rev. B **71**, 155325 (2005).
[43] S. Rodt, R. Seguin, A. Schliwa, F. Guffarth, K. Pötschke, U. Pohl, and D. Bimberg, Size-dependent binding energies and fine-structure splitting of excitonic complexes in single InAs/GaAs quantum dots, J. Lumin. **122**, 735 (2007).
[44] A. Schliwa, M. Winkelnkemper, and D. Bimberg, Few-particle energies versus geometry and composition of $In_xGa_{1-x}As$/GaAs self-organized quantum dots, Phys. Rev. B **79**, 075443 (2009).
[45] D. Thomas and J. Hopfield, Isoelectronic traps due to nitrogen in gallium phosphide, Phys. Rev. **150**, 680 (1966).
[46] M. R. Castell, D. A. Muller, and P. M. Voyles, Dopant mapping for the nanotechnology age, Nat. Mater. **2**, 129 (2003).
[47] C. F. Klingshirn, *Semiconductor Optics* (Springer, New York, 2007), Vol. 3.
[48] P. M. Koenraad and M. E. Flatté, Single dopants in semiconductors, Nat. Mater. **10**, 91 (2011).
[49] K. Sanaka, A. Pawlis, T. D. Ladd, K. Lischka, and Y. Yamamoto, Indistinguishable photons from independent semiconductor nanostructures, Phys. Rev. Lett. **103**, 053601 (2009).
[50] A. Muller, P. Bianucci, C. Piermarocchi, M. Fornari, I. C. Robin, R. André, and C. K. Shih, Time-resolved photoluminescence spectroscopy of individual Te impurity centers in ZnSe, Phys. Rev. B **73**, 081306 (2006).
[51] S. Francoeur, J. F. Klem, and A. Mascarenhas, Optical spectroscopy of single impurity centers in semiconductors, Phys. Rev. Lett. **93**, 067403 (2004).
[52] M. Ikezawa, Y. Sakuma, L. Zhang, Y. Sone, T. Mori, T. Hamano, M. Watanabe, K. Sakoda, and Y. Masumoto, Single-photon generation from a nitrogen impurity center in GaAs, Appl. Phys. Lett. **100**, 042106 (2012).
[53] L. Zhang, M. Ikezawa, T. Mori, S. Umehara, Y. Sakuma, K. Sakoda, and Y. Masumoto, Single photon generation from an impurity center with well-defined emission energy in GaAs, Jpn. J. Appl. Phys. **52**, 04CG11 (2013).
[54] G. Éthier-Majcher, P. St-Jean, G. Boso, A. Tosi, J. Klem, and S. Francoeur, Complete quantum control of exciton qubits bound to isoelectronic centres, Nat. Commun. **5**, 3980 (2014).
[55] M. Jo, T. Mano, T. Kuroda, Y. Sakuma, and K. Sakoda, Visible single-photon emission from a nitrogen impurity center in AlAs, Appl. Phys. Lett. **102**, 062107 (2013).
[56] C. Kurtsiefer, S. Mayer, P. Zarda, and H. Weinfurter, Stable solid-state source of single photons, Phys. Rev. Lett. **85**, 290 (2000).
[57] A. Beveratos, S. Kühn, R. Brouri, T. Gacoin, J.-P. Poizat, and P. Grangier, Room temperature stable single-photon source, Eur. Phys. J. D **18**, 191 (2002).
[58] V. Jacques, E. Wu, F. Grosshans, F. Treussart, P. Grangier, A. Aspect, and J.-F. Roch, Experimental realization of Wheeler's delayed-choice gedanken experiment, Science **315**, 966 (2007).
[59] S. Castelletto, I. Aharonovich, B. C. Gibson, B. C. Johnson, and S. Prawer, Imaging and quantum-efficiency measurement of chromium emitters in diamond, Phys. Rev. Lett. **105**, 217403 (2010).
[60] M. Lesik, P. Spinicelli, S. Pezzagna, P. Happel, V. Jacques, O. Salord, B. Rasser, A. Delobbe, P. Sudraud, A. Tallaire *et al.*, Maskless and targeted creation of arrays of colour centres in diamond using focused ion beam technology, Phys. Status Solidi A **210**, 2055 (2013).
[61] P. Spinicelli, A. Dréau, L. Rondin, F. Silva, J. Achard, S. Xavier, S. Bansropun, T. Debuisschert, S. Pezzagna, J. Meijer *et al.*, Engineered arrays of nitrogen-vacancy color centers in diamond based on implantation of CN-molecules through nanoapertures, New J. Phys. **13**, 025014 (2011).
[62] S. G. Cloutier, P. A. Kossyrev, and J. Xu, Optical gain and stimulated emission in periodic nanopatterned crystalline silicon, Nat. Mater. **4**, 887 (2005).
[63] D. D. Berhanuddin, M. A. Lourenço, R. M. Gwilliam, and K. P. Homewood, Co-implantation of carbon and protons: An integrated silicon device technology compatible method to generate the lasing G-center, Adv. Funct. Mater. **22**, 2709 (2012).
[64] J. Weber, H. Bauch, and R. Sauer, Optical properties of copper in silicon: Excitons bound to isoelectronic copper pairs, Phys. Rev. B **25**, 7688 (1982).
[65] H. Sumikura, E. Kuramochi, H. Taniyama, and M. Notomi, Ultrafast spontaneous emission of copper-doped silicon enhanced by an optical nanocavity, Sci. Rep. **4**, 5040 (2014).
[66] S. Castelletto, B. Johnson, V. Ivády, N. Stavrias, T. Umeda, A. Gali, and T. Ohshima, A silicon carbide room-temperature single-photon source, Nat. Mater. **13**, 151 (2014).
[67] S. Minari, L. Cavigli, F. Sarti, M. Abbarchi, N. Accanto, G. M. Matutano, S. Bietti, S. Sanguinetti, A. Vinattieri, and M. Gurioli, Single photon emission from impurity centers in AlGaAs epilayers on Ge and Si substrates, Appl. Phys. Lett. **101**, 172105 (2012).
[68] F. Sarti, G. M. Matutano, D. Bauer, N. Dotti, S. Bietti, G. Isella, A. Vinattieri, S. Sanguinetti, and M. Gurioli, Multiexciton complex from extrinsic centers in AlGaAs epilayers on Ge and Si substrates, J. Appl. Phys. **114**, 224314 (2013).
[69] N. Chand, J. Klem, T. Henderson, and H. Morkoc, Diffusion of As and Ge during growth of GaAs on Ge substrate by molecular-beam epitaxy: Its effect on the device electrical characteristics, J. Appl. Phys. **59**, 3601 (1986).
[70] R. Sieg, S. Ringel, S. Ting, E. Fitzgerald, and R. Sacks, Anti-phase domain-free growth of GaAs on offcut (001) Ge wafers by molecular beam epitaxy with suppressed Ge outdiffusion, J. Electron. Mater. **27**, 900 (1998).
[71] M. Heiss, Y. Fontana, A. Gustafsson, G. Wüst, C. Magen, D. O'Regan, J. Luo, B. Ketterer, S. Conesa-Boj, A. Kuhlmann *et al.*, Self-assembled quantum dots in a nanowire system for quantum photonics, Nat. Mater. **12**, 439 (2013).

[72] P. Corfdir, Y. Fontana, B. Van Hattem, E. Russo-Averchi, M. Heiss, A. F. i Morral, and R. Phillips, Tuning the g-factor of neutral and charged excitons confined to self-assembled (Al, Ga)As shell quantum dots, Appl. Phys. Lett. **105**, 223111 (2014).

[73] M. Ueta, K. Kanzaki, K. Kobayashi, Y. Toyozwa, and E. Hanamura, *Excitonic Processes in Solids* (Springer, Berlin, 1986), Vol. 60.

[74] L. Pavesi and M. Guzzi, Photoluminescence of $Al_xGa_{1-x}As$ alloys, J. Appl. Phys. **75**, 4779 (1994).

[75] K. Ploog, A. Fischer, and H. Künzel, The use of Si and Be impurities for novel periodic doping structures in GaAs grown by molecular beam epitaxy, J. Electrochem. Soc. **128**, 400 (1981).

[76] G. Oelgart, B. Lippold, R. Heilmann, H. Neumann, and B. Jacobs, Determination of the germanium acceptor ionisation energy of $Al_xGa_{1-x}As$ ($0 \leqslant x \leqslant 0.40$) by Hall effect and luminescence, Phys. Status Solidi A **115**, 257 (1989).

[77] P. Mooney, Deep donor levels (*DX* centers) in III-V semiconductors, J. Appl. Phys. **67**, R1 (1990).

[78] S. T. Pantelides, *Deep Centers in Semiconductors* (CRC Press, Boca Raton, FL, 1992).

[79] H. Feichtinger, in *Deep Centers in Semiconductors* (Wiley Online Library, 2008), pp. 167–229.

[80] See Supplemental Material at http://link.aps.org/supplemental/10.1103/PhysRevB.91.205316 (top part) Animated spectral map showing a 3D representation of the photoluminescence emission (the emission intensity is along z and is plotted as a function of the in-plane x and y spatial coordinates) and corresponding 2D contour plot of a sample area of 50 μm $\times$ 50 μm. The selected emission energy for these representations is shown in the bottom part of the figure with a cursor scanning on the corresponding pseudo-macro-PL spectrum.

[81] See Supplemental Material at http://link.aps.org/supplemental/10.1103/PhysRevB.91.205316 same as reference [80] but for a different sample portion.

[82] W. Bao, M. Melli, N. Caselli, F. Riboli, D. Wiersma, M. Staffaroni, H. Choo, D. Ogletree, S. Aloni, J. Bokor *et al.*, Mapping local charge recombination heterogeneity by multidimensional nanospectroscopic imaging, Science **338**, 1317 (2012).

[83] R. G. Neuhauser, K. T. Shimizu, W. K. Woo, S. A. Empedocles, and M. Bawendi, Correlation between fluorescence intermittency and spectral diffusion in single semiconductor quantum dots, Phys. Rev. Lett. **85**, 3301 (2000).

[84] A. Berthelot, I. Favero, G. Cassabois, C. Voisin, C. Delalande, P. Roussignol, R. Ferreira, and J.-M. Gérard, Unconventional motional narrowing in the optical spectrum of a semiconductor quantum dot, Nat. Phys. **2**, 759 (2006).

[85] L. Coolen, X. Brokmann, and J.-P. Hermier, Modeling coherence measurements on a spectrally diffusing single-photon emitter, Phys. Rev. A **76**, 033824 (2007).

[86] M. Abbarchi, F. Troiani, C. Mastrandrea, G. Goldoni, T. Kuroda, T. Mano, K. Sakoda, N. Koguchi, S. Sanguinetti, A. Vinattieri *et al.*, Spectral diffusion and line broadening in single self-assembled GaAs/ AlGaAs quantum dot photoluminescence, Appl. Phys. Lett. **93**, 162101 (2008).

[87] T. Mano, M. Abbarchi, T. Kuroda, C. Mastrandrea, A. Vinattieri, S. Sanguinetti, K. Sakoda, and M. Gurioli, Ultranarrow emission from single GaAs self-assembled quantum dots grown by droplet epitaxy, Nanotechnology **20**, 395601 (2009).

[88] G. Sallen, A. Tribu, T. Aichele, R. André, L. Besombes, C. Bougerol, M. Richard, S. Tatarenko, K. Kheng, and J.-P. Poizat, Subnanosecond spectral diffusion measurement using photon correlation, Nat. Photon. **4**, 696 (2010).

[89] M. Abbarchi, T. Kuroda, R. Duval, T. Mano, and K. Sakoda, Scanning Fabry-Pérot interferometer with largely tuneable free spectral range for high resolution spectroscopy of single quantum dots, Rev. Sci. Instrum. **82**, 073103 (2011).

[90] H.-S. Nguyen, G. Sallen, C. Voisin, P. Roussignol, C. Diederichs, and G. Cassabois, Optically gated resonant emission of single quantum dots, Phys. Rev. Lett. **108**, 057401 (2012).

[91] H. S. Nguyen, G. Sallen, M. Abbarchi, R. Ferreira, C. Voisin, P. Roussignol, G. Cassabois, and C. Diederichs, Photoneutralization and slow capture of carriers in quantum dots probed by resonant excitation spectroscopy, Phys. Rev. B **87**, 115305 (2013).

[92] C. Matthiesen, M. J. Stanley, M. Hugues, E. Clarke, and M. Atatüre, Full counting statistics of quantum dot resonance fluorescence, Sci. Rep. **4**, 4911 (2014).

[93] S. Marcet, R. André, and S. Francoeur, Excitons bound to te isoelectronic dyads in ZnSe, Phys. Rev. B **82**, 235309 (2010).

[94] S. Marcet, C. Ouellet-Plamondon, G. Éthier-Majcher, P. Saint-Jean, R. André, J. F. Klem, and S. Francoeur, Charged excitons and biexcitons bound to isoelectronic centers, Phys. Rev. B **82**, 235311 (2010).

[95] S. Sapra, A. Prakash, A. Ghangrekar, N. Periasamy, and D. Sarma, Emission properties of manganese-doped ZnS nanocrystals, J. Phys. Chem. B **109**, 1663 (2005).

[96] M. Abbarchi, C. Mastrandrea, T. Kuroda, T. Mano, A. Vinattieri, K. Sakoda, and M. Gurioli, Poissonian statistics of excitonic complexes in quantum dots, J. Appl. Phys. **106**, 053504 (2009).

[97] M. Abbarchi, T. Kuroda, T. Mano, K. Sakoda, C. A. Mastrandrea, A. Vinattieri, M. Gurioli, and T. Tsuchiya, Energy renormalization of exciton complexes in GaAs quantum dots, Phys. Rev. B **82**, 201301 (2010).

[98] M. Abbarchi, T. Kuroda, T. Mano, M. Gurioli, and K. Sakoda, Bunched photon statistics of the spectrally diffusive photoluminescence of single self-assembled GaAs quantum dots, Phys. Rev. B **86**, 115330 (2012).

[99] L. Cavigli, S. Bietti, N. Accanto, S. Minari, M. Abbarchi, G. Isella, C. Frigeri, A. Vinattieri, M. Gurioli, and S. Sanguinetti, High temperature single photon emitter monolithically integrated on silicon, Appl. Phys. Lett. **100**, 231112 (2012).

[100] N. Accanto, S. Minari, L. Cavigli, S. Bietti, G. Isella, A. Vinattieri, S. Sanguinetti, and M. Gurioli, Kinetics of multiexciton complex in GaAs quantum dots on Si, Appl. Phys. Lett. **102**, 053109 (2013).

[101] S. Adachi, N. Yatsu, R. Kaji, S. Muto, and H. Sasakura, Decoherence of exciton complexes in single InAlAs quantum dots measured by Fourier spectroscopy, Appl. Phys. Lett. **91**, 161910 (2007).

[102] H. Kumano, H. Kobayashi, S. Ekuni, Y. Hayashi, M. Jo, H. Sasakura, S. Adachi, S. Muto, and I. Suemune, Excitonic spin-state preservation mediated by optical-phonon resonant

excitation in a single quantum dot, Phys. Rev. B **78**, 081306 (2008).

[103] Y. Varshni, Temperature dependence of the energy gap in semiconductors, Physica **34**, 149 (1967).

[104] S. Sanguinetti, E. Poliani, M. Bonfanti, M. Guzzi, E. Grilli, M. Gurioli, and N. Koguchi, Electron-phonon interaction in individual strain-free GaAs/$Al_{0.3}Ga_{0.7}$As quantum dots, Phys. Rev. B **73**, 125342 (2006).

[105] T. Takagahara, Theory of exciton dephasing in semiconductor quantum dots, Phys. Rev. B **60**, 2638 (1999).

[106] B. Krummheuer, V. M. Axt, and T. Kuhn, Theory of pure dephasing and the resulting absorption line shape in semiconductor quantum dots, Phys. Rev. B **65**, 195313 (2002).

[107] I. Favero, G. Cassabois, R. Ferreira, D. Darson, C. Voisin, J. Tignon, C. Delalande, G. Bastard, P. Roussignol, and J. M. Gérard, Acoustic phonon sidebands in the emission line of single InAs/GaAs quantum dots, Phys. Rev. B **68**, 233301 (2003).

[108] E. A. Muljarov and R. Zimmermann, Dephasing in quantum dots: Quadratic coupling to acoustic phonons, Phys. Rev. Lett. **93**, 237401 (2004).

[109] M. Abbarchi, M. Gurioli, A. Vinattieri, S. Sanguinetti, M. Bonfanti, T. Mano, K. Watanabe, T. Kuroda, and N. Koguchi, Phonon sideband recombination kinetics in single quantum dots, J. Appl. Phys. **104**, 023504 (2008).

[110] M. Abbarchi, C. A. Mastrandrea, T. Kuroda, T. Mano, K. Sakoda, N. Koguchi, S. Sanguinetti, A. Vinattieri, and M. Gurioli, Exciton fine structure in strain-free GaAs/$Al_{0.3}Ga_{0.7}$As quantum dots: Extrinsic effects, Phys. Rev. B **78**, 125321 (2008).

[111] A. Franceschetti, H. Fu, L. W. Wang, and A. Zunger, Many-body pseudopotential theory of excitons in InP and CdSe quantum dots, Phys. Rev. B **60**, 1819 (1999).

[112] T. Tsuchiya, Biexcitons and charged excitons in quantum dots: A quantum monte carlo study, Physica E **7**, 470 (2000).

[113] D. V. Regelman, E. Dekel, D. Gershoni, E. Ehrenfreund, A. J. Williamson, J. Shumway, A. Zunger, W. V. Schoenfeld, and P. M. Petroff, Optical spectroscopy of single quantum dots at tunable positive, neutral, and negative charge states, Phys. Rev. B **64**, 165301 (2001).

[114] A. V. Filinov, C. Riva, F. M. Peeters, Y. E. Lozovik, and M. Bonitz, Influence of well-width fluctuations on the binding energy of excitons, charged excitons, and biexcitons in GaAs-based quantum wells, Phys. Rev. B **70**, 035323 (2004).

[115] G. Moody, R. Singh, H. Li, I. A. Akimov, M. Bayer, D. Reuter, A. D. Wieck, A. S. Bracker, D. Gammon, and S. T. Cundiff, Influence of confinement on biexciton binding in semiconductor quantum dot ensembles measured with two-dimensional spectroscopy, Phys. Rev. B **87**, 041304 (2013).

[116] P. Lelong and G. Bastard, Binding energies of excitons and charged excitons in GaAs/Ga(In)As quantum dots, Solid State Commun. **98**, 819 (1996).

[117] M. Abbarchi, T. Kuroda, T. Mano, K. Sakoda, and M. Gurioli, Magneto-optical properties of excitonic complexes in GaAs self-assembled quantum dots, Phys. Rev. B **81**, 035334 (2010).